

Supplementary Information for

Kinetics of Dimethyl Sulfide (DMS) Reactions with Isoprene-derived Criegee Intermediates Studied with Direct UV Absorption

Mei-Tsan Kuo,¹ Isabelle Weber,^{2,6} Christa Fittschen,² Luc Vereecken^{3,4}, Jim Jr-Min Lin^{1,5}

¹Institute of Atomic and Molecular Sciences, Academia Sinica, Taipei 10617, Taiwan

²Univ. Lille, CNRS, UMR 8522 - PC2A - Physicochimie des Processus de Combustion et de l'Atmosphère, F-59000 Lille, France

³Max Planck Institute for Chemistry, Hahn-Meitner-Weg 1, 55128 Mainz, Germany

⁴Institute for Energy and Climate Research, IEK-8: Troposphere, Forschungszentrum Jülich GmbH, 52428 Jülich, Germany

⁵Department of Chemistry, National Taiwan University, Taipei 10617, Taiwan

⁶Present address: Department of Applied Chemistry and Institute of Molecular Science, National Chiao Tung University, Hsinchu 30010, Taiwan

ORCID:

Mei-Tsan Kuo: 0000-0002-7929-9265

Jim Jr-Min Lin: 0000-0002-8308-2552

Christa Fittschen: 0000-0003-0932-432X

Isabelle Weber: 0000-0001-5142-4557

Luc Vereecken: 0000-0001-7845-684X

S1 Summary of the experimental conditions and results

Table S1. Summary of the experimental conditions and results for the reaction CH₂OO+DMS at 308 nm photolysis. $T = 296.8\text{--}297.2$ K; $[\text{O}_2] = (3.28\text{--}3.32)\times 10^{17}$ cm⁻³; $P_{\text{total}} = 299.9\text{--}301.5$ Torr.

Exp#	[CH ₂ I ₂] /10 ¹³ cm ⁻³	$I_{308\text{nm}}$ /mJ cm ⁻²	k_0 /s ⁻¹	k_{DMS} /10 ⁻¹⁶ cm ³ s ⁻¹
1	16.1	1.19	232±2 ^a	7.8±4.1 ^a
2	16.3	2.35	464±3	10.9±5.6
3	16.2	3.63	698±3	22.0±5.5
4	16.5	4.83	956±5	-4.1±10.4
5	12.6	0.34	54±2	9.1±4.5
6	21.2	0.31	79±2	10.2±4.1
7	20.7	0.31	90±2	8.6±4.9
8	21.1	0.74	188±1	-3.2±1.7
9	19.6	0.95	240±2	12.0±3.5
10	2.30	9.97	261±8	28.7±16.7
11	25.4	2.27	680±4	24.1±8.2
average				11.5
standard deviation ^b				10.3

^a averaged value ± 1 sigma error of the mean (statistical only, not including systematic errors). Note: 1 sigma error of the mean = standard deviation / sqrt(degrees of freedom)

^b Standard deviation of the 11 data points of k_{DMS} .

Table S2. Summary of the experimental conditions and results for the reaction CH₂OO+DMS at 248 nm photolysis. $T = 296.7\text{K--}296.8$ K; $[\text{O}_2] = 3.29\times 10^{17}$ cm⁻³; $P_{\text{total}} = 299.5\text{--}299.7$ Torr.

Exp#	[CH ₂ I ₂] /10 ¹³ cm ⁻³	$I_{248\text{nm}}$ /mJ cm ⁻²	k_0 /s ⁻¹	k_{DMS} /10 ⁻¹⁶ cm ³ s ⁻¹
12	19.3	1.10	109±1 ^a	16.2±10.3 ^a
13	19.0	2.18	197±1	25.5±8.6
14	18.9	3.17	275±1	31.6±11.5
average				24.4
standard deviation ^b				7.8

^a averaged value ± 1 sigma error of the mean (statistical only, not including systematic errors). Note: 1 sigma error of the mean = standard deviation / sqrt(degrees of freedom)

^b Standard deviation of the 3 data points of k_{DMS} .

Table S3. Summary of the experimental conditions and results for the reaction MVKO + DMS at 248 nm photolysis. $T = 297.0\text{--}298.1\text{ K}$; $[\text{O}_2] = (3.28\text{--}3.41)\times 10^{17}\text{ cm}^{-3}$.

Exp#	Precursor	P_{total} /Torr	$I_{248\text{nm}}$ /mJ cm ⁻²	k_r /s ⁻¹	adduct yield		
	Abs				$1-\alpha$ /%	k_0 /s ⁻¹	k_{DMS} /10 ⁻¹⁶ cm ³ s ⁻¹
15	0.100	301.4	1.09	1182±14 ^b	91.8±0.3 ^b	115±2 ^b	116.5±34.3 ^b
16	0.220	303.0	1.06	1442±7	89.2±0.1	151±2	94.7±34.5
17	0.331	301.6	1.03	1641±5	87.2±0.1	182±2	73.2±24.0
18	0.334	301.9	0.58	1386±10	90.4±0.2	140±1	99.9±19.1
19	0.056	302.1	1.25	1033±48	91.1±1.6	123±8	75.0±70.7
20	0.151	302.2	1.23	1109±14	91.2±0.3	131±2	44.2±22.5
21	0.057	302.5	2.45	1203±14	90.6±0.2	146±2	19.6±17.0
22	0.158	302.3	2.43	1395±6	87.0±0.1	179±5	78.7±56.1
23	0.056	302.3	3.72	1330±5	88.9±0.3	229±2	33.2±15.9
24	0.160	302.4	3.67	1652±8	84.0±0.1	274±1	-15.0±16.7
25	0.179	30.6	1.19	1297±7	57.0±0.2	138±2	70.3±58.1
26	0.558	30.2	1.14	2123±19	49.2±0.1	255±2	67.8±59.3
27	0.289	100.2	1.18	1481±12	79.2±0.2	153±1	68.4±7.7
28	0.746	99.9	1.11	2146±8	70.7±0.1	321±2	39.6±25.8
29	0.142	299.5	1.19	1362±11	88.7±0.1	126±1	57.1±14.8
average							61.6
standard deviation ^c							33.4

^a The estimated absorbance of the precursor (1,3-diiodo-2-butene) at 238 nm in the photolysis reactor (using $L = 426\text{ cm}$).

^b averaged value ± 1 sigma error of the mean (statistical only, not including systematic errors).

Note: 1 sigma error of the mean = standard deviation / sqrt(degrees of freedom)

^c Standard deviation of the 15 data points of k_{DMS} .

S2 Observed decay rate coefficient of CH₂OO at various conditions

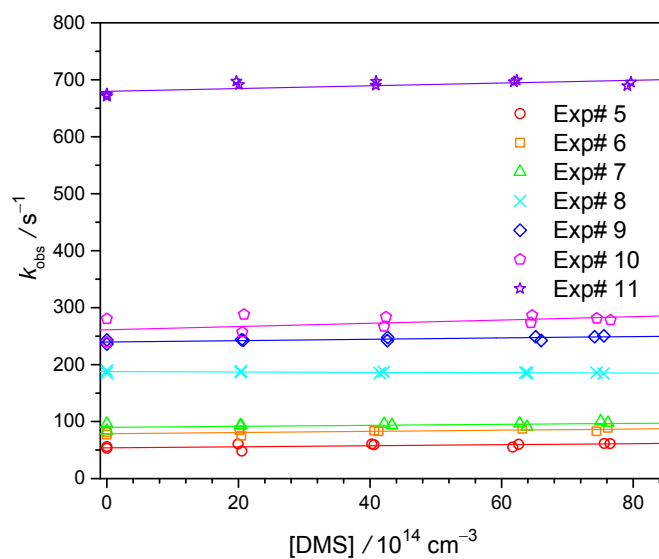


Fig. S1. First-order decay rate coefficient of CH₂OO, k_{obs} , against [DMS] at various experimental conditions (Exp#5–11, Table S1). The wavelength of the photolysis laser is 308 nm.

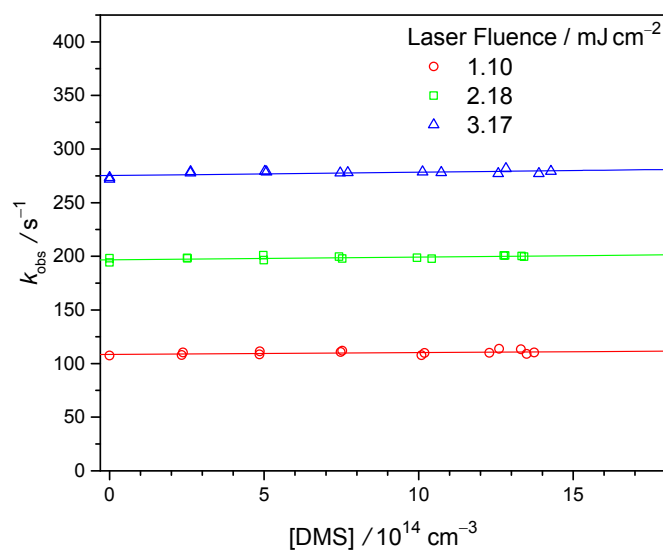
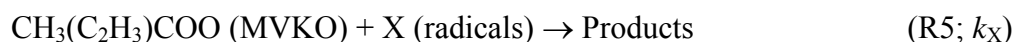
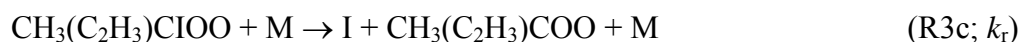


Fig. S2. First-order decay rate coefficient of CH₂OO, k_{obs} , against [DMS] at various photolysis laser fluence (Exp#12–14, Table S2). The wavelength of the photolysis laser is 248 nm.

S3 Kinetic model for MVKO reactions

To obtain more quantitative values for k_{DMS} , we performed kinetic analysis with the following model. At $t = 0$, the precursor $\text{ICH}_2\text{-CH=C(I)-CH}_3$ is photodissociated into $\text{CH}_3(\text{C}_2\text{H}_3)\text{CI} + \text{I}$. Under the high $[\text{O}_2]$ conditions ($\sim 3.3 \times 10^{17} \text{ cm}^{-3}$) in our experiment, the reaction of $\text{CH}_3(\text{C}_2\text{H}_3)\text{CI} + \text{O}_2$ (R3a) and (R3b) proceeds within a very short time ($< 0.1 \text{ ms}$). However, different from the case of CH_2OO , an additional MVKO signal rises slowly until about 2 ms (R3c), followed by a decay in longer reaction times (due to (R4) and (R5)). The formation/decomposition of the adduct of MVKO and I atom (R3b)/(R3c) are pressure dependent.



The detail kinetics of the adduct decomposition into MVKO + I will be published elsewhere. In brief, MVKO is either formed directly (R3a), or via the formation and consecutive decomposition of an adduct of $\text{CH}_3(\text{C}_2\text{H}_3)\text{CIOO}$ ((R3b) and (R3c)). From the differential rate equations of these three reactions, the following analytical expression for $[\text{MVKO}](t)$ can be derived:

$$\begin{aligned} [\text{MVKO}](t) &= [\text{MVKO}]_0 e^{-k_{\text{obs}}t} + [\text{adduct}]_0 \frac{k_{\text{r}}}{k_{\text{r}} - k_{\text{obs}}} [e^{-k_{\text{obs}}t} - e^{-k_{\text{r}}t}] \\ &= [\text{MVKO}]_{\text{total}} \left\{ \alpha e^{-k_{\text{obs}}t} + (1-\alpha) \frac{k_{\text{r}}}{k_{\text{r}} - k_{\text{obs}}} [e^{-k_{\text{obs}}t} - e^{-k_{\text{r}}t}] \right\} \end{aligned} \quad (3)$$

with α and $(1-\alpha)$ as the yields of the prompt MVKO and the adduct ($[\text{MVKO}]_{\text{total}} = [\text{MVKO}]_0 + [\text{adduct}]_0$) and $k_{\text{obs}} = k_0 + k_{\text{DMS}}[\text{DMS}]$ as in the case of CH_2OO . Fitting this equation to the measured absorbance–time profiles treating k_{obs} , k_{r} , and α as variable parameters, we obtained k_{obs} . Selected results of k_{obs} are presented in Figure 4 and all results are summarized in Table S3.

S4 Observed decay rate coefficient of MVKO at various conditions

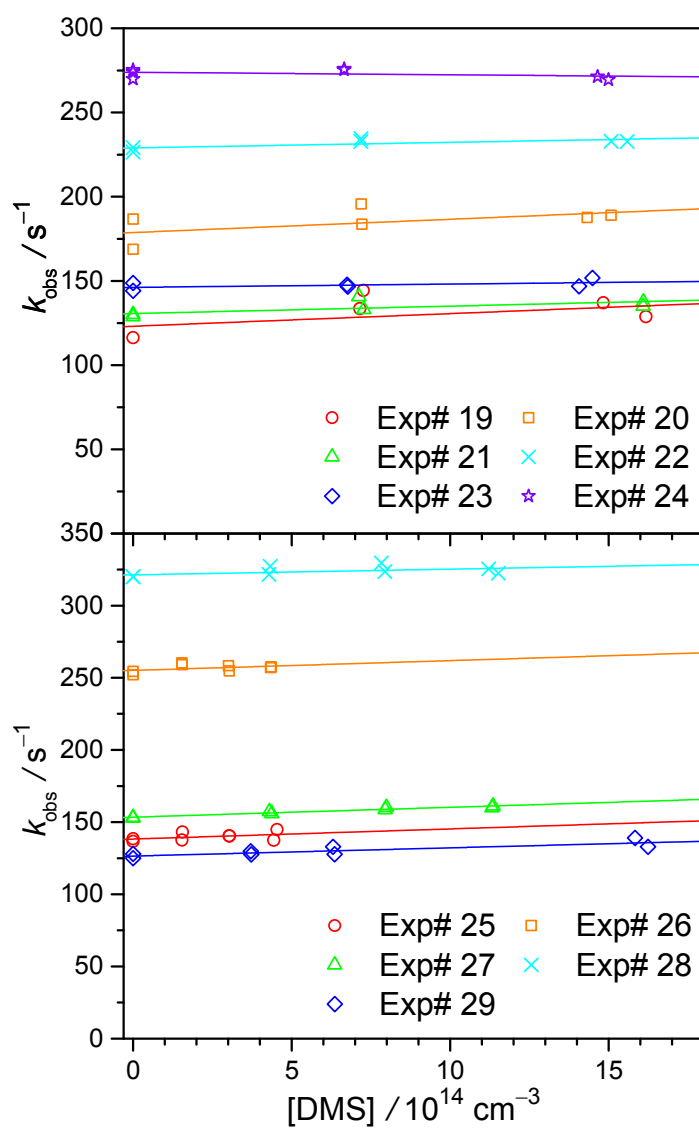


Fig. S3. First-order decay rate coefficient of MVKO, k_{obs} , against $[\text{DMS}]$ at various experimental conditions (Exp#19–29). The wavelength of the photolysis laser is 248 nm.

S5 Effect of DMS photolysis

Assuming the photolysis yield of DMS is unity, the concentration of the photodissociated DMS, $[\text{DMS}]_{\text{diss}}$, can be deduced from the following equation:

$$[\text{DMS}]_{\text{diss}} = [\text{DMS}] \rho \sigma$$

$$\rho = I \frac{\lambda}{hc}$$

where $\rho = I\lambda/hc$ is the number of photons per unit area and σ is the absorption cross section of DMS; I and λ are the fluence and wavelength of the photolysis laser; h and c are the Planck constant and speed of light, respectively. The maximum values of photodissociated DMS and CH_2I_2 precursor are estimated as in Table S4.

Table S4. Estimation for the photodissociated DMS and CH_2I_2 .

Wavelength	I / mJ cm^{-2}	ρ / cm^{-2}	σ / cm^2	$[\text{DMS}]_{\text{diss}}/[\text{DMS}]$	$[\text{DMS}]$ / cm^{-3}	$[\text{DMS}]_{\text{diss}}$ / cm^{-3}
248 nm	3.72	4.64×10^{15}	1.28×10^{-20}	5.9×10^{-5}	1.7×10^{15}	1.0×10^{11}
308 nm	9.97	1.55×10^{16}	$< 1 \times 10^{-22}$	$< 1.5 \times 10^{-6}$	8.1×10^{15}	$< 1.3 \times 10^{10}$

				$[\text{CH}_2\text{I}_2]_{\text{diss}}/[\text{CH}_2\text{I}_2]$	$[\text{CH}_2\text{I}_2]$ / cm^{-3}	$[\text{CH}_2\text{I}_2]_{\text{diss}}$ / cm^{-3}
248 nm	3.17	3.96×10^{15}	1.6×10^{-18}	6.3×10^{-3}	1.9×10^{14}	1.2×10^{12}
308 nm	9.97	1.55×10^{16}	3.3×10^{-18}	5.1×10^{-2}	2.3×10^{13}	1.2×10^{12}

High $[\text{DMS}]_{\text{diss}}$ at 248 nm photolysis would generate radical products, which may react with CH_2OO or MVKO and may absorb light at our probe wavelength (see **Figure S4**). On the other hand, the very minor $[\text{DMS}]_{\text{diss}}$ at 308 nm photolysis would not cause a problem. Hence, at 248 nm photolysis, we limit $[\text{DMS}] \leq 1.7 \times 10^{15} \text{ cm}^{-3}$ and $I_{248\text{nm}} \leq 3.72 \text{ mJ cm}^{-2}$ (Exp#23–24) to constraint $[\text{DMS}]_{\text{diss}} \leq 1.0 \times 10^{11} \text{ cm}^{-3}$. **Figure S5** shows the background trace at 248 nm photolysis with constraint $[\text{DMS}]$ and $I_{248\text{nm}}$. No significant background due to $[\text{DMS}]_{\text{diss}}$ is observed, except absorption caused from the optics. Besides, in **Figure S9**, we can see that the results of $\text{CH}_2\text{OO} + \text{DMS}$ reaction at 248 nm photolysis are quite similar to those at 308 nm, while a slightly higher k_{DMS} can be observed for 248 nm at high $I_{248\text{nm}}$, indicating that $[\text{DMS}]_{\text{diss}}$ only has a minor effect.

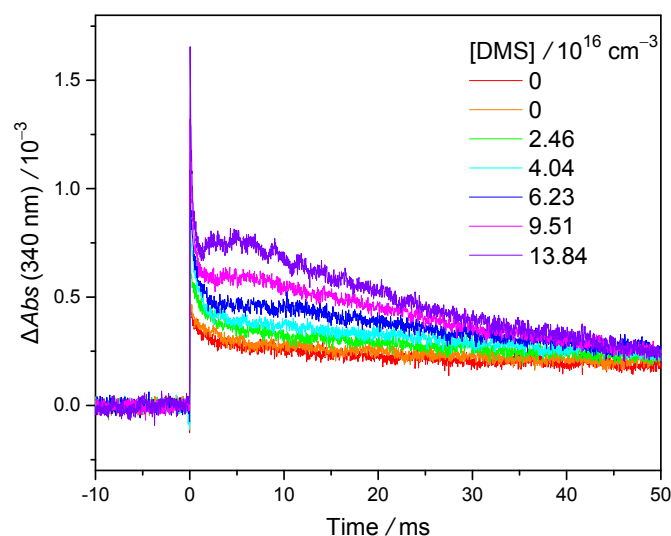


Fig. S4. Background traces recorded under extra-high [DMS]. The traces were obtained with 248 nm photolysis laser ($I_{248\text{nm}} = 3.34 \text{ mJ cm}^{-2}$). The experimental conditions are : $P_{\text{total}} = 297.2 \text{ Torr}$, $[\text{O}_2] = 3.23 \times 10^{17} \text{ cm}^{-3}$, $T = 299 \text{ K}$. The length of the cell for monitoring [DMS] is 1 cm. The photolysis laser pulse defines $t = 0$. The absorbance change under zero [DMS] comes from the interaction of the optics and the photolysis laser pulse. Note that in the kinetic experiments, the used [DMS] was much lower ($< 1.7 \times 10^{15} \text{ cm}^{-3}$) such that the background did not depend on [DMS] (see Figure S5).

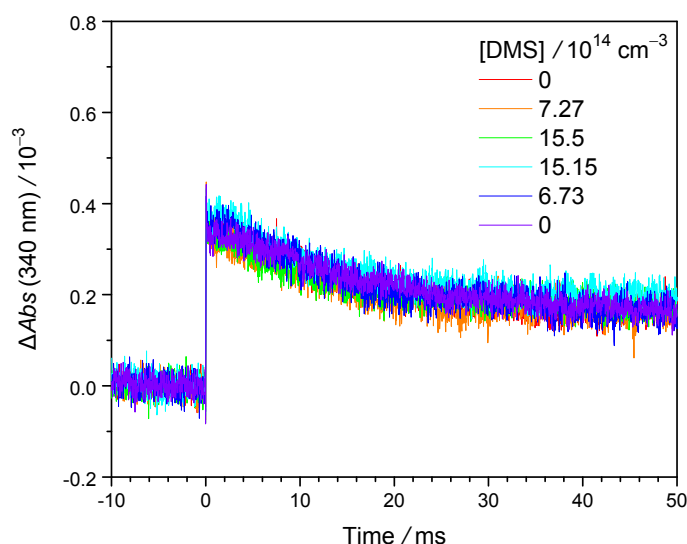


Fig. S5. Background traces under normal DMS concentrations obtained with 248 nm photolysis laser ($I_{248\text{nm}} = 3.72 \text{ mJ cm}^{-2}$). See Exp# 23 of Table S3 for the experimental condition.

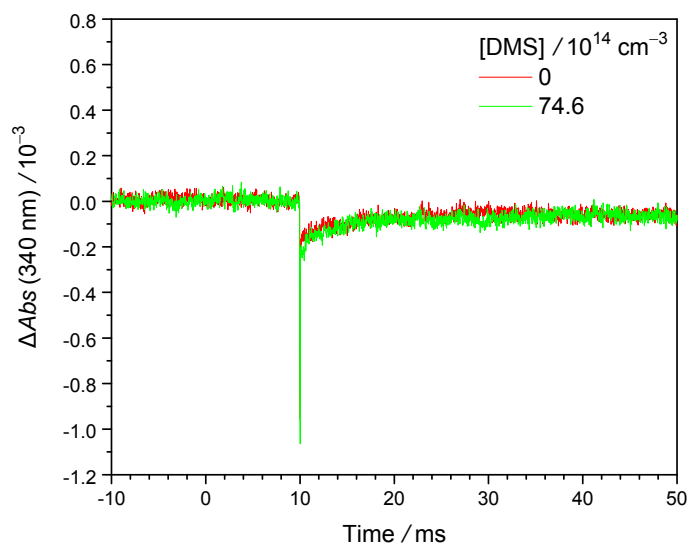


Fig. S6. Background traces under various [DMS] obtained with 308 nm photolysis laser ($I_{308\text{nm}} = 4.83\text{ mJ cm}^{-2}$). See Exp#4 of Table S1 for the experimental condition. Note that the optics (long pass filters) are different from those at 248 nm.

S6 Dependence of k_0 and k_{DMS} on laser fluence and precursor concentration

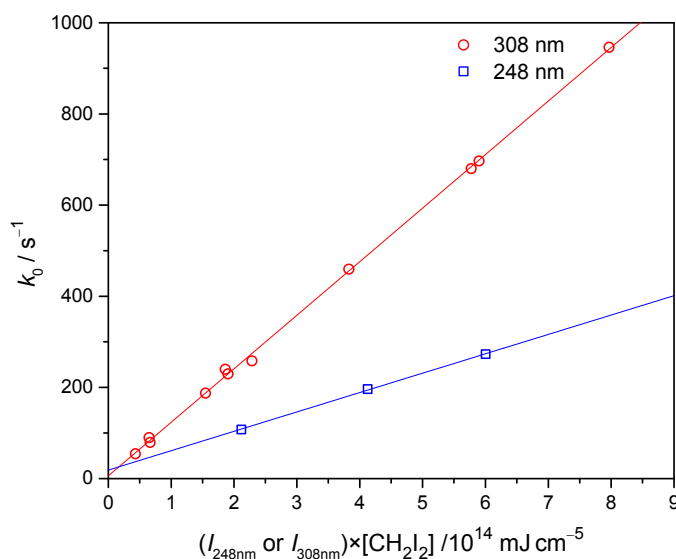


Fig. S7. Plot of k_0 against the product of the laser fluence ($I_{248\text{nm}}$ or $I_{308\text{nm}}$) and the precursor concentration $[\text{CH}_2\text{I}_2]$ for the experiments (Exp#1–14, Tables S1–S2) of $\text{CH}_2\text{OO} + \text{DMS}$ reaction. The x-axis essentially represents the total amounts of radical species generated through the photolysis of the precursor (R1) and the subsequent reactions (R2). Higher radical concentration results in faster CH_2OO decay, thus higher k_0 . The difference of the slopes mainly comes from the difference of CH_2I_2 absorption cross sections at these two wavelengths (see Table S4). Note that there are experiments having different combinations of $[\text{CH}_2\text{I}_2]$ and $I_{308\text{nm}}$, but very similar $I_{308\text{nm}} \times [\text{CH}_2\text{I}_2]$ (like Exp#3,11; Exp#1,9).

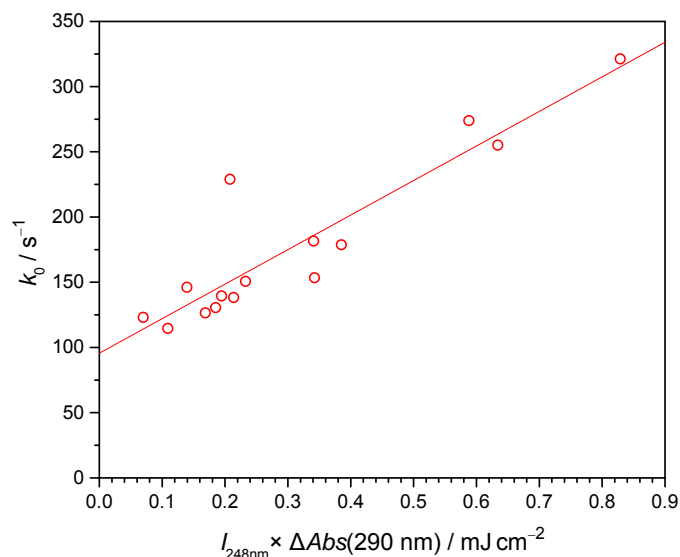


Fig. S8. As Figure S7, but for the experiments (Exp#15–29) of MVKO+DMS reaction. Because the absorption cross section of the precursor is not available, we use its absorbance to represent its concentration.

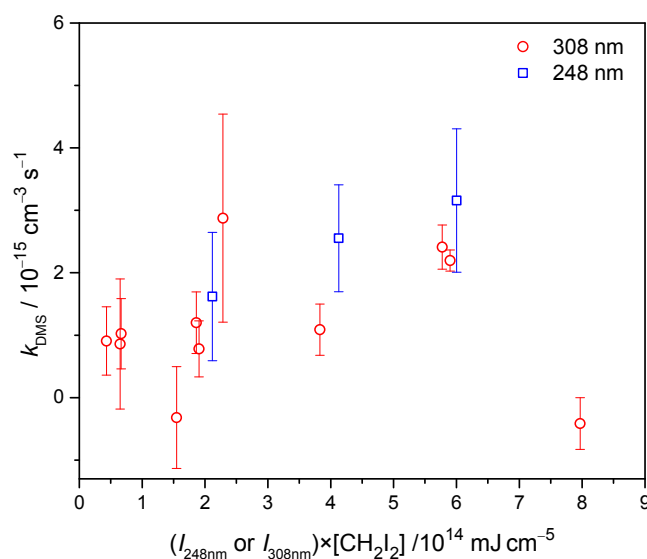


Fig. S9. Plot of k_{DMS} against the product of the laser fluence ($I_{248\text{nm}}$ or $I_{308\text{nm}}$) and the precursor concentration $[\text{CH}_2\text{I}_2]$ for the experiments (Exp#1–14, Tables S1–S2) of $\text{CH}_2\text{OO}+\text{DMS}$ reaction. The x-axis essentially represents the total amounts of radical species generated through the photolysis of the precursor (R1) and the subsequent reactions (R2). No observable trend of k_{DMS} can be found for the data of 308 nm photolysis, whereas k_{DMS} at 248 nm photolysis increases as $I_{248\text{nm}} \times [\text{CH}_2\text{I}_2]$ increases, which may result from the increased radical generation from the DMS photolysis. Note that there are experiments having different combinations of $[\text{CH}_2\text{I}_2]$ and $I_{308\text{nm}}$, but very similar $I_{308\text{nm}} \times [\text{CH}_2\text{I}_2]$ (like Exp#3,11; Exp#1,9).

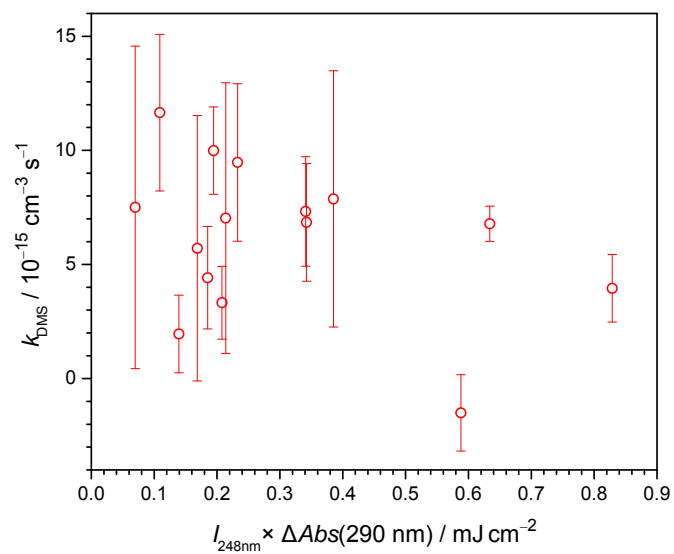


Fig. S10. As Figure S9, but for k_{DMS} in Exp#15–29 of MVKO+DMS reaction. No significant trend for k_{DMS} is observed.

S7 Representative time traces for the $\text{CH}_2\text{OO} + \text{DMS}$ reaction obtained with 308 nm photolysis

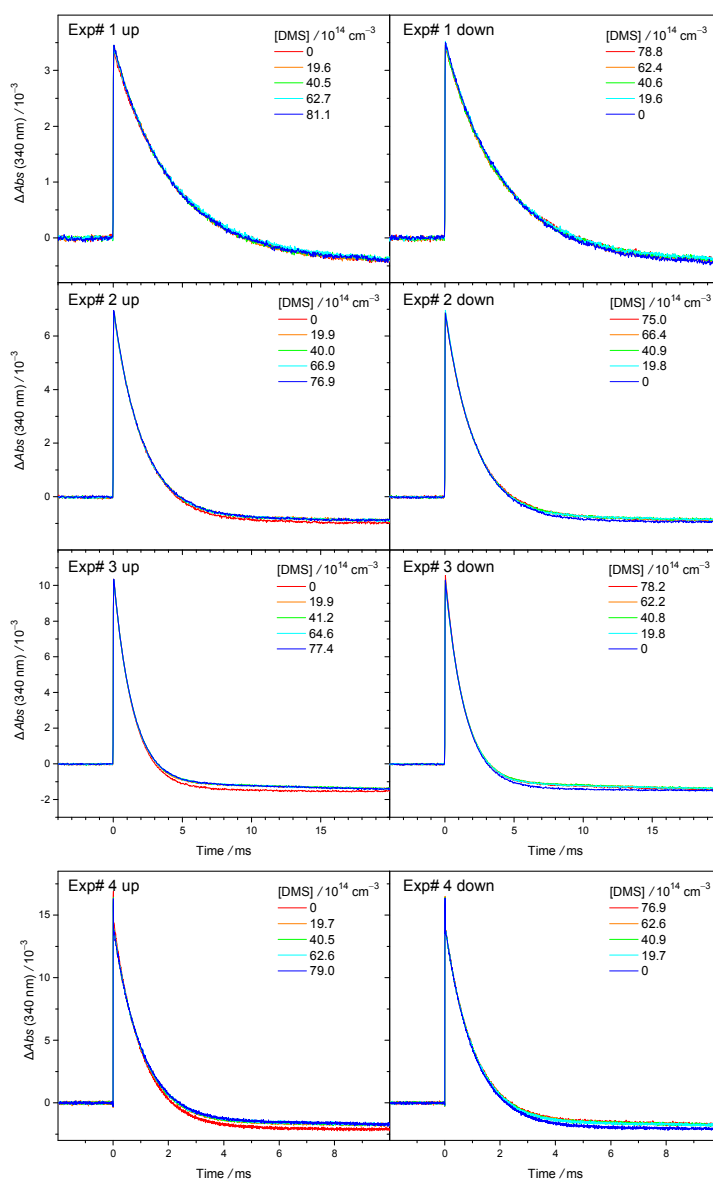


Fig. S11. Representative time traces of CH_2OO absorption at $340 \pm 5 \text{ nm}$ at various $[\text{DMS}]$ (Exp#1–4). The wavelength of the photolysis laser was 308 nm and the laser pulse is set at the time zero. In each experiment, $[\text{DMS}]$ was scanned from 0 to the maximum (labeled as “up”), and scanned from maximum to 0 (labeled as “down”). The negative baseline is resulted from the depletion of the precursor CH_2I_2 .

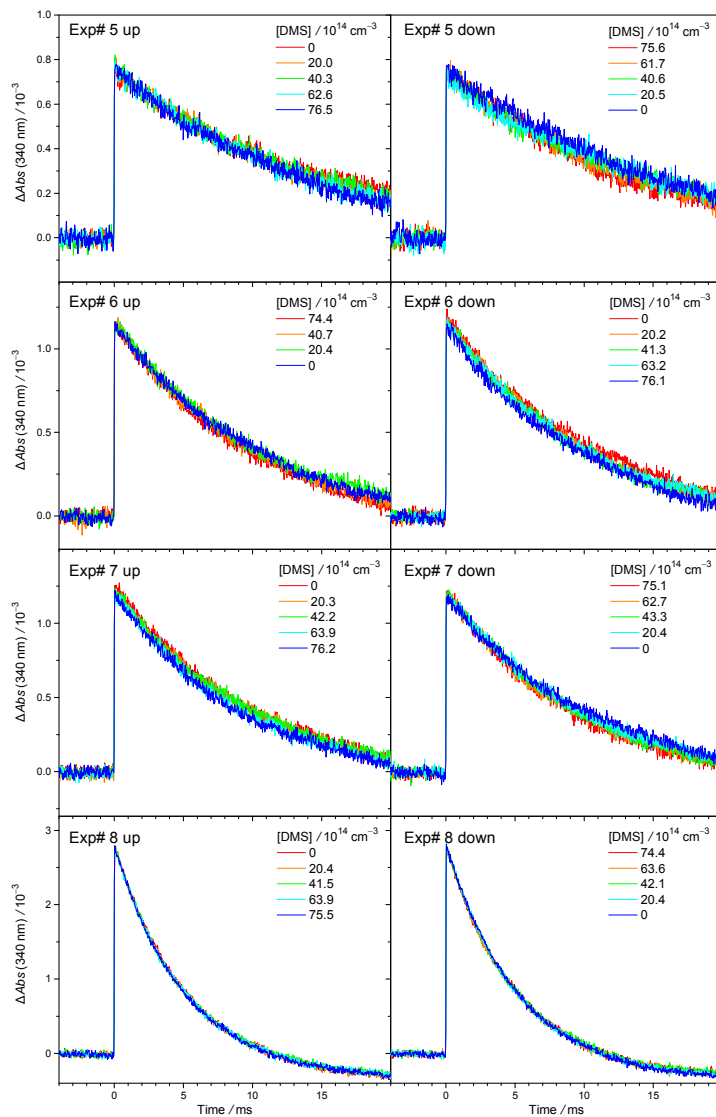


Fig. S12. As Fig. S11, but different experiment sets (Exp#5–8)

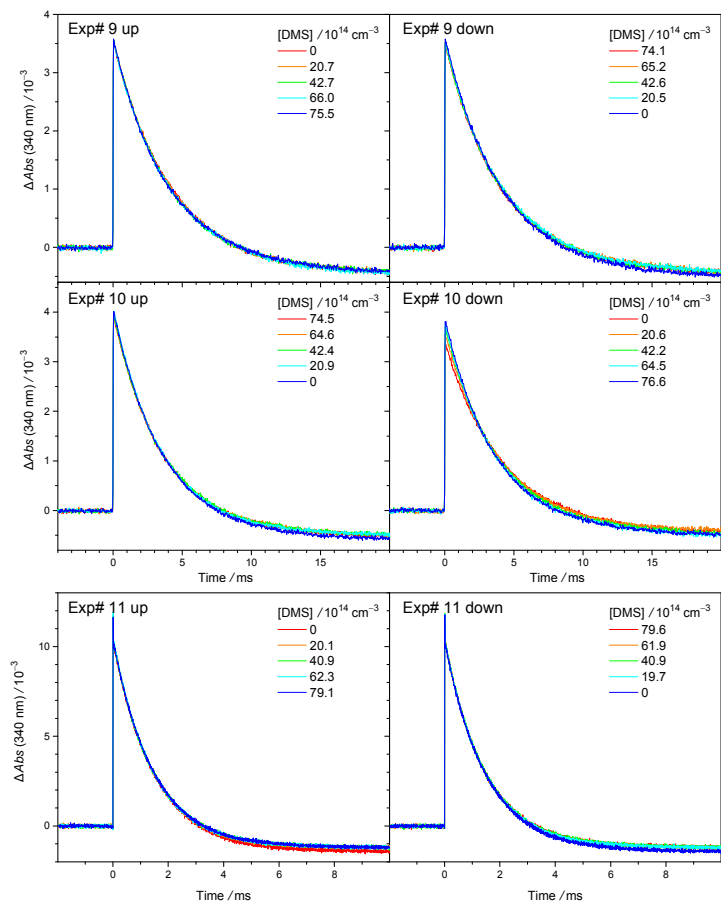


Fig. S13. As Fig. S11, but different experiment sets (Exp#9–11)

S8 Representative time traces for the CH₂OO+DMS reaction obtained with 248 nm photolysis

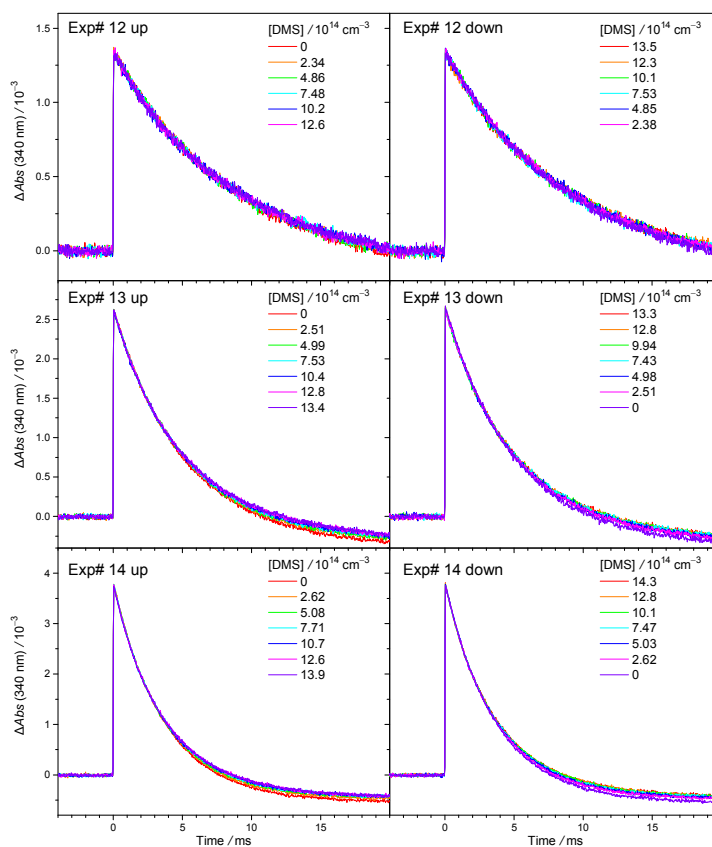


Fig. S14. Representative time traces of CH₂OO at 340±5nm at various [DMS] (Exp# 12–14). The wavelength of the photolysis laser was 248 nm and the laser pulse is set at the time zero. In each experiment, [DMS] was scanned from 0 to the maximum (labeled as “up”), and scanned from maximum to 0 (labeled as “down”). The negative baseline resulted from the depletion of the precursor CH₂I₂.

S9 Representative time traces for the MVKO+DMS reaction obtained with 248 nm photolysis

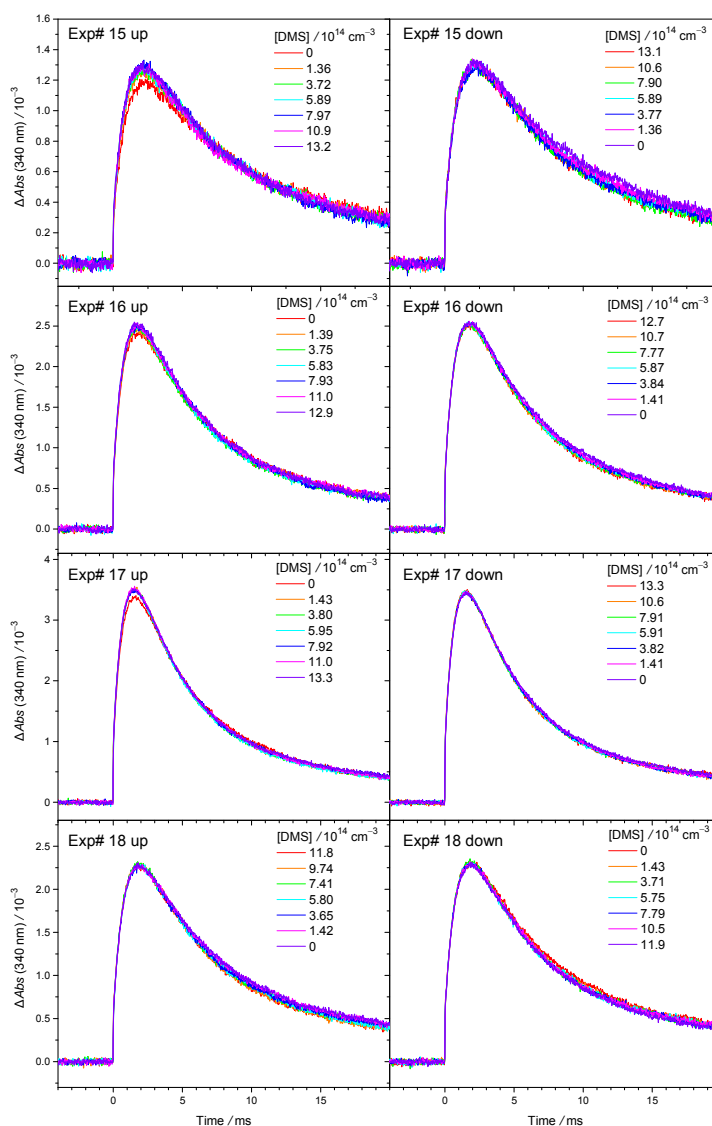


Fig. S15. Representative time traces of MVKO at 340±5nm at various [DMS] (Exp#15–18). The wavelength of the photolysis laser was 248 nm and the laser pulse is set at the time zero. In each experiment, [DMS] was scanned from 0 to the maximum (labeled as “up”), and scanned from maximum to 0 (labeled as “down”).

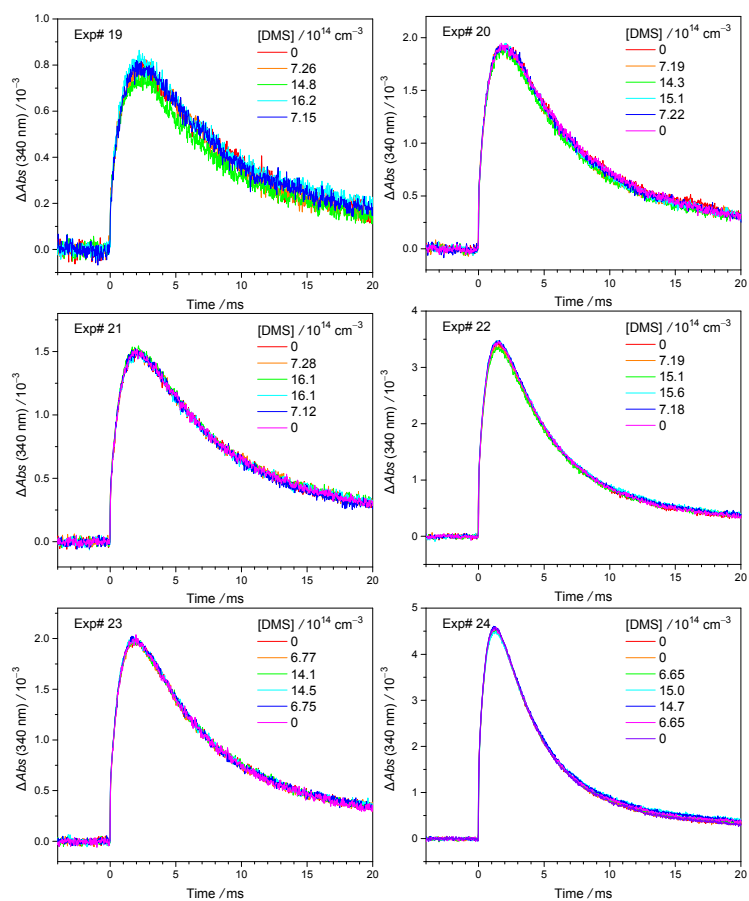


Fig. S16. Representative time traces of MVKO at $340\pm 5\text{ nm}$ at various [DMS] (Exp#19–24). The wavelength of the photolysis laser was 248 nm and the laser pulse is set at the time zero.

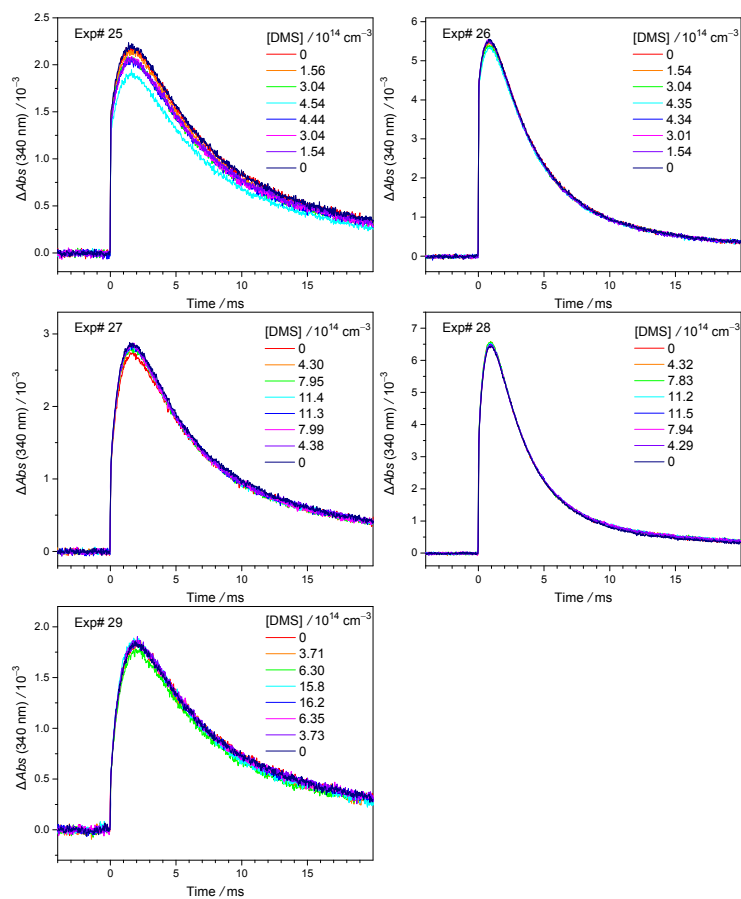


Fig. S17. As Fig. S16, but different experiment sets (Exp#25–29)

S10 Computational details for the reaction of CH₂OO + DMS

Additional methodological information

The CH₂OO + DMS system was characterized at the CCSD(T)/aug-cc-pVTZ//M06-2X/aug-cc-pV(T+d)Z level of theory. Though the computational demands of the reaction system prevent us from doing higher-level calculations at this time, this level of theory is expected to be sufficient to give a good idea of the PES layout, and derive rate coefficients with an accuracy of about one to two orders of magnitude. In particular, the study by Newland et al. (2015) proposes a very fast reaction which should then have a low energy barrier, whereas the current experimental study finds very slow elementary reactions which perforce must have a high energy barrier. The level of theory applied is able to easily discriminate between these extreme cases.

An additional set of exploratory calculations were performed at the M06-2X/cc-pVDZ level of theory, specifically on DMS + larger CI, DMS + CH₂OO in the presence of O₂, and unimolecular reactions of CH₂OO, *syn*-CH₃CHOO, *anti*-CH₃CHOO, and *cyc*-CH₂OOS(O)O- with and without complexation with DMS. These calculations at lower level are discussed here in the supporting information. For these calculations, only relative barrier heights on analogous reactions are important, which are sufficiently well described at the level of theory employed. As no indication for a significant enhancing effect on the reaction rate was found, no attempt was made to improve the absolute barrier heights.

Impact of substitutions of the CI, or the presence of O₂, on the CI + DMS reaction

Calculations for CH₂OO + DMS + O₂ reveal no influence of O₂ as a reaction partner, though the (CH₃)₂SCH₂OO adduct may form a complex with O₂ stabilized by few kcal mol⁻¹. O₂ addition on the (CH₃)₂SCH₂OO and CH₃S(=CH₂)CH₂OOH adducts, forming triplet peroxy radicals, was found to have large barriers exceeding 15 kcal mol⁻¹, and is not competitive against redissociation of the CI+DMS adducts even at atmospheric O₂ concentrations.

Calculations on the reactions of *syn*-CH₃CHOO and *anti*-CH₃CHOO with DMS show that, as opposed to the CH₂OO case, formation of (CH₃)₂SCH(CH₃)OO adducts is endothermic by a few kcal mol⁻¹, making reaction of substituted CI with DMS even less favorable. This conclusion is expected to hold also for the MVKO CI.

DMS as a catalyst

The experiments of Newland et al. (2015) found no evidence of DMS consumption, suggesting that the DMS activity hampering SO₂ oxidation by CI in their isoprene + O₃ system might be caused by catalytic effects. Hence, we examined whether the unimolecular decay of CI could be affected by complexation with DMS, performing a set of calculations using the lower level M06-2X/cc-pVDZ level of theory. At that level of theory, the complexes of CH₂OO,

syn-CH₃CHOO and *anti*-CH₃CHOO with DMS are stabilized by 8.5 to 10.9 kcal mol⁻¹ (likely overestimated due to basis set superposition errors). The barriers for dioxirane formation in CH₂OO, *syn*-CH₃CHOO and *anti*-CH₃CHOO are 22.0, 25.8 and 18.4 kcal mol⁻¹ without DMS, respectively, while in the DMS complex they are 24.1, 26.8 and 20.4 kcal mol⁻¹ above the complex, respectively. In *syn*-CH₃CHOO, the energy barrier for 1,4-H-migration (vinylhydroperoxide channel) without and with DMS are 12.7 and 15.8 kcal mol⁻¹, respectively, again calculated from the bottom of the CI-DMS complex. These results, despite being at a less reliable level of theory, strongly suggest that the DMS complexation does not lower the intrinsic barriers for unimolecular rearrangements, and might even slightly increase them. Any catalytic effect of DMS on the unimolecular decomposition of CI is then due to the energy release of the complexation, but this is insufficient to lower the decay TS close to or below the energy level of free CI + DMS, such that the main fate of the complex remains redissociation without chemical loss. This is in agreement with the observations of the current experimental study, which sees no enhanced CI loss in the presence of DMS.

There are many other reactions in the isoprene + O₃ system that might be catalytically enhanced or slowed by DMS, and examining all of these is outside the scope of this study. We did examine the reaction of DMS with the adduct of CH₂OO + SO₂, *i.e.* the thio-secondary ozonide (*cyc*-CH₂OOS(O)O-, thio-SOZ) (Kuwata et al., 2015; Vereecken et al., 2012) formed prior to its decomposition to SO₃ + CH₂O. The DMS-catalyzed redissociation of thio-SOZ back to CH₂OO + SO₂, thus inhibiting SO₂ oxidation by CI, was found at the M06-2X/cc-pVDZ level of theory to have an energy barrier of 17.8 kcal mol⁻¹, too high to compete against SO₃ formation for which a barrier ≤ 10 kcal mol⁻¹ was found (Kuwata et al., 2015). Any inhibiting effect by DMS on the CI + SO₂ reaction is thus not caused by an enhanced redissociation of the thio-SOZ intermediate.

No data is available elucidating whether bimolecular reactions of CI-DMS complexes with suitable co-reactants (SO₂, H₂O, acids,...), or alternatively DMS complexes of such co-reactants with free CI, are hindered or enhanced relative to those of the free CI + co-reactant.

References

Kuwata, K. T., Guinn, E., Hermes, M. R., Fernandez, J., Mathison, J. and Huang, K.: A Computational Re-Examination of the Criegee Intermediate-Sulfur Dioxide Reaction, *J. Phys. Chem. A*, 119(41), 10316–10335, doi:10.1021/acs.jpca.5b06565, 2015.

Newland, M. J., Rickard, A. R., Vereecken, L., Muñoz, A., Ródenas, M. and Bloss, W. J.: Atmospheric isoprene ozonolysis: impacts of stabilised Criegee intermediate reactions with

SO₂, H₂O and dimethyl sulfide, *Atmospheric Chem. Phys.*, 15(16), 9521–9536, doi:10.5194/acp-15-9521-2015, 2015.

Vereecken, L., Harder, H. and Novelli, A.: The reaction of Criegee intermediates with NO, RO₂, and SO₂, and their fate in the atmosphere, *Phys. Chem. Chem. Phys.*, 14(42), 14682–14695, doi:10.1039/c2cp42300f, 2012.